Potential energy surface and bound states of the NH3–Ar and ND3–Ar complexes

J. Loreau, J. Liévin, Y. Scribano, and A. van der Avoird

Citation: The Journal of Chemical Physics **141**, 224303 (2014); doi: 10.1063/1.4903047
View online: http://dx.doi.org/10.1063/1.4903047
View Table of Contents: http://scitation.aip.org/content/aip/journal/jcp/141/22?ver=pdfcov
Published by the AIP Publishing

Articles you may be interested in

Rovibrational energy transfer in the He-C3 collision: Potential energy surface and bound states
J. Chem. Phys. **140**, 084316 (2014); 10.1063/1.4866839

Interaction of the NO 3pπ Rydberg state with Ar: Potential energy surfaces and spectroscopy
J. Chem. Phys. **138**, 214313 (2013); 10.1063/1.4808027

A new ab initio intermolecular potential energy surface and predicted rotational spectra of the Ar−H2S complex
J. Chem. Phys. **136**, 084310 (2012); 10.1063/1.3689443

Ab initio intermolecular potential energy surface, bound states, and microwave spectra for the van der Waals complex Ne–HCCCN
J. Chem. Phys. **122**, 174312 (2005); 10.1063/1.1888567

Potential energy surface and rovibrational states of the ground Ar–HI complex
J. Chem. Phys. **120**, 6471 (2004); 10.1063/1.1665467

This article is copyrighted as indicated in the article. Reuse of AIP content is subject to the terms at: http://scitation.aip.org/termsconditions. Downloaded to IP: 164.15.19.51 On: Mon, 08 Dec 2014 14:51:09

Potential energy surface and bound states of the NH_3–Ar and ND_3–Ar complexes

J. Loreau,[1,a)] J. Liévin,[1] Y. Scribano,[2] and A. van der Avoird[3]
[1]*Service de Chimie Quantique et Photophysique, Université Libre de Bruxelles (ULB) CP 160/09, 50 av. F.D. Roosevelt, 1050 Brussels, Belgium*
[2]*Laboratoire Univers et Particules de Montpellier, Université de Montpellier II, LUPM – UMR CNRS 5299, 34095 Montpellier Cedex, France*
[3]*Theoretical Chemistry, Institute for Molecules and Materials, Radboud University Nijmegen, Heyendaalseweg 135, 6525 AJ Nijmegen, The Netherlands*

(Received 17 October 2014; accepted 19 November 2014; published online 8 December 2014)

A new, four-dimensional potential energy surface for the interaction of NH_3 and ND_3 with Ar is computed using the coupled-cluster method with single, double, and perturbative triple excitations and large basis sets. The umbrella motion of the ammonia molecule is explicitly taken into account. The bound states of both NH_3–Ar and ND_3–Ar are calculated on this potential for total angular momentum values from $J = 0$ to 10, with the inclusion of Coriolis interactions. The energies and splittings of the rovibrational levels are in excellent agreement with the extensive high-resolution spectroscopic data accumulated over the years in the infrared and microwave regions for both complexes, which demonstrates the quality of the potential energy surface. © *2014 AIP Publishing LLC*. [http://dx.doi.org/10.1063/1.4903047]

I. INTRODUCTION

The interaction of ammonia with noble gases (NG) has been the subject of a large number of studies motivated mainly by the understanding of weak interactions[1] as well as by the importance of rotational energy transfer in NH_3–NG collisions in the modelling of various astrophysical and atmospherical environments.[2] Moreover, the possibility of producing cold and ultracold NH_3 molecules either by buffer gas cooling or by sympathetic cooling with noble gas atoms has been examined.[3]

The NH_3–Ar van der Waals (vdW) complex has been the subject of extensive microwave and far infrared spectroscopic studies. The first measurements on the complex were performed in the microwave region[4,5] and resulted in a complicated spectrum due to the nonrigidity of the complex. Additional transitions were observed and assigned in the microwave and infrared for *ortho*[6–8] and *para*[8–10] NH_3–Ar, which showed that for some states ammonia behaves almost as a free rotor in the complex. These spectroscopic investigations have resulted in a precise knowledge of the bound states of the complex that correlate to the $j_k = 0_0$, 1_0, and 1_1 levels of free NH_3, including states with vibrational excitation in the van der Waals stretching coordinate. In addition to the rotational constants, the dipole moment and the nuclear quadrupole splitting constants have also been reported for some states. These studies have been complemented by the observation of transitions in the $\nu_1 + \nu_3$ band region of the complex[11] as well as spectroscopic measurements on the rotational states of ND_3–Ar.[12–14]

Several potential energy surfaces (PES) have been developed over the years in order to help the understanding of the spectrum of the complex. The first PES was constructed using Møller-Plesset perturbation theory up to second order (MP2).[15] An improved, semi-empirical surface developed by Bulski *et al.* included the dependence of the potential on the umbrella inversion angle.[16] This PES was used to compute the bound states of the complex[17–19] including the effects of the inversion motion. While important discrepancies with the experimental data were observed, it was noted that these could be partly resolved by scaling a single term in the expansion of the PES by a constant factor. Integral and differential cross sections for rotational excitation and inversion of NH_3 in collisions with Ar were also computed with this potential,[20–23] and reasonable agreement with experimental data was found. A third PES developed at the MP4 level by Tao and Klemperer[24] confirmed the main features of the previous intermolecular potential. The most recent PES was obtained by Schmuttenmaer *et al.*[25] by fitting the spectroscopic data, which provided a detailed understanding of the spectrum of the complex. Finally, geometry optimization calculations were performed recently by Bistoni *et al.*[26] using the coupled cluster method, in relation with molecular beam experiments probing the isotropic part of the PES,[1] with good agreement between theory and experiment.

Recently, the interaction of NH_3 and ND_3 with noble gases has found a renewed interest due to the possibility of measuring state-selective differential cross sections corresponding to rotationally and inversion inelastic collisions in a crossed beam setup with hexapole selected[27,28] or Stark-decelerated ammonia,[29] combined with velocity-map imaging. A direct comparison between theory and these recent experiments requires a more accurate PES that includes the umbrella inversion motion explicitly, which is the subject of the present work.

a)jloreau@ulb.ac.be

 © 2014 AIP Publishing LLC

This article is copyrighted as indicated in the article. Reuse of AIP content is subject to the terms at: http://scitation.aip.org/termsconditions. Downloaded to IP: 164.15.19.51 On: Mon, 08 Dec 2014 14:51:09

In Sec. II, we describe a new four-dimensional (4D) PES obtained using the coupled cluster method and a large basis set. We discuss the features of the PES; we found that it is in good agreement with the experimentally determined PES.[25] In Sec. III, we describe the calculation of the spectrum of the van der Waals complex using the new PES. We compute the band origins, rotational constants, and inversion tunneling splittings of the rovibrational states of NH_3–Ar and ND_3–Ar and compare these with the spectroscopic data.

II. POTENTIAL ENERGY SURFACE

A. Methods

We constructed a 4-dimensional PES, which depends on the three spherical coordinates (R', θ', φ') used to define the Ar atom position with respect to NH_3, as well as on the NH_3 umbrella angle ρ', which describes the inversion motion of ammonia. The C_{3v} symmetry of ammonia is retained, and ρ' is the angle between the C_3 axis of NH_3 and the NH bonds. The Ar position vector $\mathbf{R}'$ is defined relative to the N atom, R' is the length of $\mathbf{R}'$, θ' (with $0 \le \theta' \le \pi$) is the angle between the vector $\mathbf{R}'$ and the C_3 axis, and φ' (with $0 \le \varphi' \le 2\pi$) is the angle of rotation of this vector around the C_3 axis. When $\theta' = 0$ or π, the complex has orientation Ar–NH_3 or Ar–H_3N, respectively. An angle $\varphi' = 0$ corresponds to Ar in the same plane as the C_3 axis and one of the NH bonds, while for $\varphi' = \pi/3$ Ar is located at equal distance between two hydrogen atoms.

We can easily transform to a coordinate system (ρ, R, θ, φ) with the origin set at the center of mass of NH_3, which will be required for bound states and scattering calculations. The umbrella angle ρ and the angle φ are left unchanged by this transformation ($\rho' = \rho$, $\varphi' = \varphi$) while the internuclear distance R and angle θ are related to R' and θ' by

$$\begin{aligned} \theta &= \operatorname{arccot}\left(\cot\theta' - \frac{z_{cm}}{R'\sin\theta'}\right), \\ R &= \frac{R'\sin\theta'}{\sin\theta}, \end{aligned} \tag{1}$$

where

$$z_{cm} = \frac{3m_H}{M} r\cos\rho \tag{2}$$

is the distance from the N nucleus to the center of mass of NH_3, and $M = m_N + 3m_H$ is the mass of NH_3. Similarly, we can define a coordinate system with the origin set at the center of mass of ND_3 by using Eq. (1) and replacing m_H by m_D in Eq. (2). The coordinate system is illustrated in Fig. 1.

The N–H distance r was kept fixed to its vibrationally averaged value r_0 in the ground vibrational state of NH_3. Since NH_3 keeps its C_{3v} symmetry, the three NH bonds remain equally long. The value of r_0 can be obtained from the rotational constants B_0 and C_0 of NH_3, for which accurate values are available experimentally.[30] The relationship between the rotational constants and r_0 can be found using the principal moments of inertia of NH_3, $I_{xx} = I_{yy} = 3m_H r^2(1/2\sin^2\rho + m_N/M\cos^2\rho)$ and $I_{zz} = 3m_H r^2\sin^2\rho$ and the fact that $B_0 = \hbar/2I_{xx}$ and $C_0 = \hbar/2I_{zz}$. Using the values of Ref. 30 for B_0 and C_0 averaged over the inversion tunneling states, we get r_0 = 1.9204 a_0 and $\rho_0 = 111.4°$. These can be compared to the equilibrium values, $r_e = 1.9099\ a_0$ and $\rho_e = 112.1°$.[31]

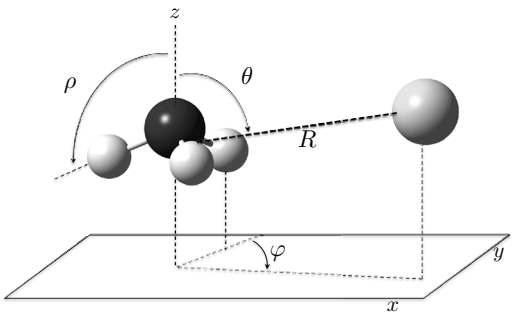

FIG. 1. Coordinate system for NH_3–Ar with the origin at the center of mass of NH_3.

The ground state PES of the NH_3–Ar complex was computed by means of the coupled-cluster method with single, double, and perturbative triple excitations (CCSD(T))[32] with a Hartree-Fock reference wave function, as implemented in the MOLPRO 2012.1 package.[33] For states with monoconfigurational character, the CCSD(T) method provides the best compromise between accuracy and computation time. For each geometry, the energy was corrected for the basis set superposition error by means of the counterpoise method.[34]

In order to select the basis set appropriate to NH_3–Ar, we performed a series of calculations using variants of the aug-cc-pVnZ (or AVnZ) basis sets for various cardinal numbers n at several geometries $\mathbf{x}_i$. The results are reported in Table I for two geometries $\mathbf{x}_1$, close to the global minimum of the PES, and $\mathbf{x}_2$, located in the long range. The second column of Table I contains the BSSE-corrected interaction energies computed using the AVnZ ($n = 2 - 5$) basis sets on all atoms.[35,36] The $2s^2 2p^3$ electrons of the N atom, the $1s$ electrons of the H atoms, and the $3s^2 3p^6$ electrons of the Ar atom, i.e., 16 electrons in total, were correlated in the CCSD(T) calculations. We also computed the Complete Basis Set (CBS) limit of the interaction energy. The CBS energies were obtained by extrapolating the Hartree-Fock energy and the correlation energy separately using the standard approach.[37]

TABLE I. Energy of the complex (in cm^{-1}) for the two geometries $\mathbf{x}_1$ ($\rho = 112°$, $R' = 6.8\ a_0$, $\theta' = 90°$, $\varphi = 60°$) and $\mathbf{x}_2$ ($\rho = 100°$, $R' = 12\ a_0$, $\theta' = 150°$, $\varphi = 40°$) and for various basis sets (see text). AVnZ is a shorthand notation for aug-cc-pVnZ.

	n	AVnZ	AVnZ-mb	AVnZ-DK-mb	ACVnZ-mb
$\mathbf{x}_1$	2	−80.445	−152.06	−152.51	−151.62
	3	−123.79	−147.19	−147.62	−147.31
	4	−138.83	−146.56	−146.99	−146.95
	5	−143.81	−146.91	−147.33	−147.27
	CBS	−148.81			
$\mathbf{x}_2$	2	−6.1725	−7.3344	−7.3456	−7.3212
	3	−6.9242	−7.4101	−7.4211	−7.3820
	4	−7.1334	−7.3539	−7.3645	−7.3269
	5	−7.2402	−7.3478	−7.3581	−7.3199
	CBS	−7.3612			

This article is copyrighted as indicated in the article. Reuse of AIP content is subject to the terms at: http://scitation.aip.org/termsconditions. Downloaded to IP: 164.15.19.51 On: Mon, 08 Dec 2014 14:51:09

Specifically, a three-parameter exponential function was used for the HF energy, while a two-parameter n^{-3} form was employed to extrapolate the correlation energy. The basis sets with cardinal number $n = 3 - 5$ were used in this procedure. Following the extrapolation, the energy was corrected for the BSSE error.

It is well known that the description of weakly interacting complexes can be improved by the inclusion of a set of diffuse functions located midway between the two fragments. We adopted a set of $(3s3p2d2f1g)$ mid-bond functions[38] which has been shown to give accurate results for noble gases. The results obtained with the AVnZ basis set supplemented with mid-bond functions, denoted as AVnZ-mb, are given in the third column of Table I. We observe that for both geometries the AVQZ-mb results are in good agreement with the CBS limit and are better than the AV5Z results. The CBS extrapolation cannot be performed with the AVnZ-mb basis sets as the addition of mid-bond functions breaks the hierarchy of the basis sets, as can be seen from Table I.

The interaction energy can be further improved by including scalar relativistic effects. These corrections were taken into account using the Douglas-Kroll-Hess Hamiltonian[39] and the adapted basis sets AVnZ-DK,[40] as well as their mid-bond functions – augmented versions AVnZ-DK-mb. We observe that such corrections increase the stability of the complex and improve the interaction energy by 0.5% at most, as can be seen from the fourth column of Table I. The effect of relativistic corrections is found to be the same without the mid-bond functions (not shown). Similar trends were reported for acetylene-noble gas complexes.[41]

Finally, we investigated the effect of opening the cores of the atoms by using the aug-cc-pCVnZ (or ACVnZ) basis sets[42,43] augmented by mid-bond functions (ACVnZ-mb). Core-valence interactions can indeed alter the interaction energy significantly for heavy noble gases.[44] Twenty-six electrons were correlated in these calculations, which become prohibitively expensive with large basis sets. As can be seen from the last column of Table I, the effect is rather small (less than 0.4%) and can be neglected. The order of magnitude of the effect is the same without the mid-bond functions (not shown).

The tests presented above were also performed at two other geometries $\mathbf{x}_3$ and $\mathbf{x}_4$ in the short range and in the interaction region (not shown), which led to the same conclusions. We therefore selected the AVQZ-DK-mb basis to compute the full PES of the complex.

The PES was generated from 6820 geometries. A grid of 31 points in R' was used in the interval from 4 to $30\,a_0$. A spacing of 0.5 a_0 for $4 \le R' \le 6a_0$ and 0.3 a_0 for $6 \le R' \le 6.6a_0$ was selected in the repulsive region. In the region close to the minimum (between 6.6 and $7.8\,a_0$), we used a constant grid spacing of $0.2\,a_0$, and the spacing gradually increases for larger R'. The grid over θ' was chosen as a Gauss-Legendre grid with 11 points from 0 to π, while for φ' we used a Gauss-Chebyshev grid of 4 points from 0 to $\pi/3$. The grid over ρ' was constructed with five points, with a constant spacing given by $(2\rho_0 - \pi)/5$. The potential for other geometries can be obtained by symmetry. The complete set of *ab initio* points is available as the supplementary material.[45] The T1 diagnostic[46] was less than 0.009 for all geometries, which confirms the mono-reference character of the wave function all over the PES and justifies the use of the CCSD(T) method for the NH_3–Ar complex.

In order to obtain an analytic representation of the potential, we first expanded it in tesseral harmonics

$$V(R, \theta, \varphi, \rho) = \sum_{l,m} v_{lm}(R, \rho) S_{lm}(\theta, \varphi). \tag{3}$$

The tesseral harmonics S_{lm} are real-valued combinations of spherical harmonics Y_{lm}, the $m > 0$ functions being of cosine type. The sum over l runs from $l = 0$ to 10, which is allowed since the θ-grid contains 11 points, while the sum over m runs from 0 to l. Due to the threefold symmetry, only terms for which m is a multiple of 3 appear in the expansion of the potential. The expansion coefficients $v_{lm}(R, \rho)$ in Eq. (3) can be computed at all grid points R_i and ρ_j by numerically integrating the product of the potential and the corresponding expansion functions $S_{lm}(\theta, \varphi)$ over the angles θ and φ, which is straightforward as the potential was calculated at Gauss-Legendre and Gauss-Chebyshev quadrature points.

The representation of the functions $v_{lm}(R, \rho)$ is different in the interaction region (defined as $R \le 30\ a_0$) and in the asymptotic region ($R > 30\ a_0$). In the interaction region, the functions $v_{lm}(R, \rho)$ were fitted using two-dimensional cubic splines. To estimate the quality of the fit, we calculated the relative root mean square (RMS) deviation as well as the relative deviation of the fit on the complete grid of *ab initio* energies. The former is defined as the RMS error divided by the mean interaction energy, while the latter is the mean deviation of the fit for all grid points. The RMS deviation was found to be 0.42% while the relative deviation was 0.025%, which establishes the quality of the spherical expansion. In order to test the fit in R and ρ, we computed the potential energy at 30 additional points. For the points located in the short-range region of the potential, we found a relative error of about 3% while in the intermediate and long-range regions the relative error was less than 0.3%.

The functions $v_{lm}(R, \rho)$ in the asymptotic region were constructed by fitting the three outermost points in the R-grid to an expansion in inverse powers of R and a polynomial expansion in ρ, similar to what was done for NH_3–He[29]

$$v_{lm}(R, \rho) = \sum_{n,p} c_{lmnp} \left(\rho - \frac{\pi}{2}\right)^p R^{-n}. \tag{4}$$

We kept only the first two terms in the inverse R-power expansion, $n = n_i$ and $n = n_i + 2$. The value of n_i depends[47] on the value of l: $n_i = 6$ for $l = 0$ and 2, while $n_i = 7$ for $l = 1$ and 3, and $n_i = l + 4$ for $l \ge 4$. We included ten terms in the polynomial expansion in ρ, with p taking values from 0 to 9. However, the functions $v_{lm}(R, \rho)$ are even or odd functions of $(\rho - \pi/2)$ according to the parity of $l + m$, so that only terms with p even or odd appear in the sum. Each function $v_{lm}(R, \rho)$ is thus represented by 10 coefficients c_{lmnp}. The analytic form (4) for the asymptotic v_{lm} functions was used for the first 9 functions, corresponding to all couples (lm) with $l < 6$.

This article is copyrighted as indicated in the article. Reuse of AIP content is subject to the terms at: http://scitation.aip.org/termsconditions. Downloaded to IP: 164.15.19.51 On: Mon, 08 Dec 2014 14:51:09

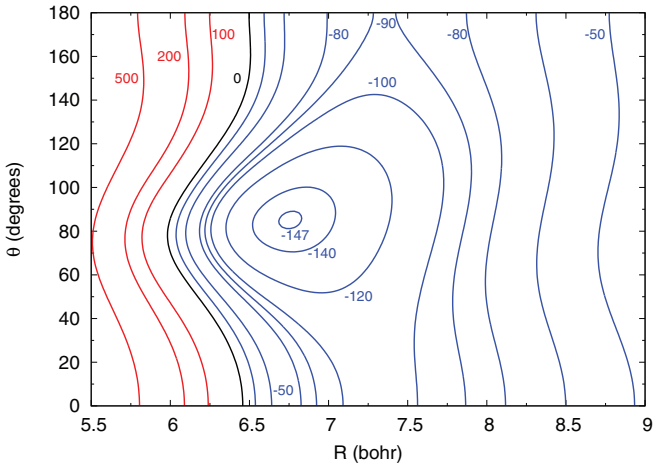

FIG. 2. Contour plot of the PES (in cm^{-1}) for $\varphi = 60°$, $\rho = \rho_e$.

B. Results

The features of the PES are illustrated in Figs. 2–4 by two-dimensional cuts for the equilibrium value of the NH_3 umbrella angle, $\rho_e = 112.1°$. Figs. 2 and 3 show cuts in R and θ for $\varphi = 60°$ and $\varphi = 0°$, respectively. As illustrated in Fig. 2, we find that the global minimum of the surface is located at $R = 6.756\ a_0$, $\theta = 85.1°$, and $\varphi = 60°$ with a corresponding well depth of $D_e = 147.64\ cm^{-1}$. The equilibrium geometry is shown in Fig. 1. The preferred orientation of the complex has Ar between two hydrogen atoms ($\varphi = 60°$) and slightly above the nitrogen atom ($\theta = 85.1°$). These values are compared in Table II to those previously obtained with the MP2[15] and MP4[24] methods, as well as with the semi-empirical PES of Bulski *et al.*[16] and the PES of Schmutzenmaer *et al.* obtained by fitting the observed transitions.[25] We observe that the well depth of our potential as well as the equilibrium geometry are almost identical to those obtained from the fit to experiment.

When Ar is rotated around the C_3 axis to $\varphi = 0$, the minimum is shifted to $R = 7.20\ a_0$, $\theta = 74.2°$ and the corresponding energy is $-118.1\ cm^{-1}$. When $\varphi = 0$, the Ar atom is in the plane formed by the C_3 axis and one of the N–H bonds,

TABLE II. Comparison of the parameters of the global minimum of the PES with previous works. The coordinates used in Ref. 15 have the origin on the N atom and have been transformed using Eq. (1). The coordinates used in Refs. 24 and 25 are related to our coordinates through the transformation $\theta \to \pi - \theta$.

	MP2[15]	MP4[24]	Semi-empirical[16]	Expt.[25]	This work
D_e (cm^{-1})	115.0	130.1	134.2	149.6	147.6
R_e (a_0)	7.110	6.857	6.780	6.746	6.756
θ_e (deg)	79.0	90.0	75.0	83.4	85.1
φ_e (deg)	60	60	60	60	60

and it cannot approach NH_3 as closely as for $\varphi = 60°$ so that the equilibrium distance is increased. The barrier preventing internal rotation along the φ coordinate is 29.5 cm^{-1}, to be compared with the value of 25.6 cm^{-1} deduced from experimental data.[10]

It is interesting to note that the long-range behavior of the PES is quite different for $\varphi = 0$ and for $\varphi = 60°$. For $\varphi = 0$, we observe in Fig. 3 that for fixed R the minimum is along $\theta = 112°$. This particular angle corresponds to Ar approaching along one of the N–H bonds, which maximizes the dispersion interaction. However, this structure is the least favorable at short range so that the minimum shifts progressively towards lower values of θ when R is decreased. For $\varphi = 60°$ (Fig. 2), the minimum is located along $\theta = 0$ in the long-range (Ar above N), and another minimum can be seen for $\theta = 135°$. When R is decreased the second orientation becomes more favorable while θ decreases to its equilibrium value θ_e.

Figure 4 shows a cut of the PES in R and φ for $\theta = \theta_e$ and $\rho = \rho_e$. We observe again that the orientation with $\varphi = 0$ minimizes the interaction energy in the long range, while $\varphi = 60°$ is preferred in the short range.

We can also compare the two symmetric top configurations of the complex, i.e., $\theta = 0$ and $\theta = 180°$. For $\theta = 0$ (Ar–NH_3 configuration), the minimum is located at $R = 7.31\ a_0$ with an energy of $-103.6\ cm^{-1}$, 44 cm^{-1} above the global minimum. For $\theta = 180°$ (NH_3–Ar configuration), the minimum is located at $R = 7.35\ a_0$ with an energy of $-90.1\ cm^{-1}$, 57.5 cm^{-1} above the global minimum. The first structure

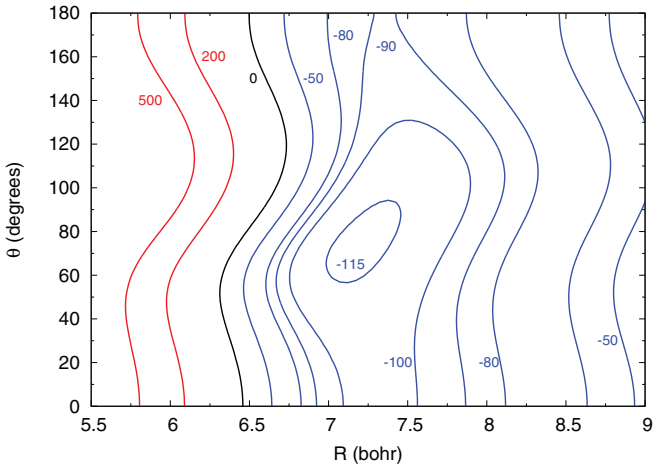

FIG. 3. Contour plot of the PES (in cm^{-1}) for $\varphi = 0°$, $\rho = \rho_e$.

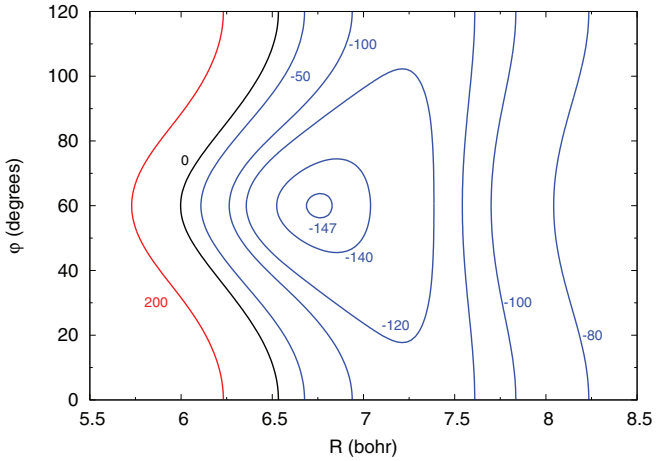

FIG. 4. Contour plot of the PES (in cm^{-1}) for $\theta = 85.1°$, $\rho = \rho_e$.

This article is copyrighted as indicated in the article. Reuse of AIP content is subject to the terms at: http://scitation.aip.org/termsconditions. Downloaded to IP: 164.15.19.51 On: Mon, 08 Dec 2014 14:51:09

is therefore more favorable, and the difference in energy of 13.5 cm^{-1} between the two configurations shows that the double well potential of free NH_3 is perturbed by Ar. This will affect the inversion tunneling splitting in the rovibrational states of the complex.

III. BOUND STATES

A. Theory

The molecular symmetry group of NH_3–Ar with inversion motion is $D_{3h}(M)$. This group is isomorphic to D_{3h} and is the same as for free NH_3. Therefore, the allowed rovibrational states and their statistical weights are also identical. We recall[17,48] that due to the symmetry of the total wavefunction, which should be antisymmetric under an odd fermion permutation, it can be shown that the irreducible representations A_2' and A_2'' have statistical weight 12 (ortho states), the representations E' and E'' have weight 6 (para states), and the A_1' and A_1'' have weight 0. Levels corresponding to the A_1 representations thus are absent from the spectra. The rotational states of NH_3 are labeled by the quantum numbers j and k, where j is the angular momentum of ammonia and k is its projection on the C_3 axis. States with $k = 0$ (modulo 3) correspond to ortho states, while those with $k = \pm 1$ (modulo 3) correspond to para states. In addition, for $k = 0$ and odd j only states that are symmetric with respect to inversion are present while for even j only antisymmetric states are allowed.[48] As the interaction that mixes para and ortho states is negligibly small, they can be considered independently in spectroscopic and collisional studies.

The Hamiltonian of the system can be written as[19]

$$\hat{H} = \hat{H}_a - \frac{\hbar^2}{2\mu R}\frac{\partial^2}{\partial R^2}R + \frac{1}{2\mu R^2}(\hat{J}^2 + \hat{j}^2 - 2\hat{\mathbf{j}}\cdot\hat{\mathbf{J}}) + V(\rho, R, \theta, \varphi), \quad (5)$$

where μ is the reduced mass of the system, $\hat{\mathbf{j}}$ is the space-fixed angular momentum operator of NH_3, and $\hat{\mathbf{J}}$ is the body-fixed total angular momentum operator. The Hamiltonian $\hat{H}_a$ of the NH_3 molecule is given by

$$\hat{H}_a = \sum_i \frac{\hat{j}_i^2}{2I_{ii}(\rho)} + \hat{T}(\rho) + V(\rho), \quad (6)$$

where $i = x, y, z$, and the I_{ii} are the corresponding principal moments of inertia given in Sec. II A. The operator $\hat{T}(\rho)$ is the kinetic operator for the curvilinear umbrella motion,[19] while $V(\rho)$ describes the double well potential of NH_3 in the ρ coordinate. We used the analytical representation of $V(\rho)$ given in Ref. 29, which reproduces accurately the experimental tunneling frequencies (0.79 cm^{-1} and 35.2 cm^{-1}, respectively) in the ground ($v = 0$) and first excited ($v = 1$) umbrella vibrational states, as well as the $v = 0 \rightarrow 1$ excitation frequency of 949.9 cm^{-1}. The umbrella potential $V(\rho)$ for ND_3 was fitted similarly. The corresponding tunneling splittings are much smaller, 0.0530 cm^{-1} and 3.50 cm^{-1}, and the vibrational frequency is also smaller, 747.3 cm^{-1}, but the resulting double well potential differs only slightly from that of NH_3.

The Hamiltonian is diagonal in the quantum numbers J (total angular momentum) and M (its projection on the space-fixed z axis). The projection Ω of J (also called K) on the van der Waals bond axis $\mathbf{R}$ would be an exact quantum number if the terms $\hat{j}_+\hat{J}_+$ and $\hat{j}_-\hat{J}_-$ in the Coriolis coupling operator $\hat{\mathbf{j}}\cdot\hat{\mathbf{J}}$ in Eq. (5) were neglected. These terms mix states with $\Delta\Omega = \pm 1$ but are usually small, so that the rotational states of the complex may still be labeled with the value of Ω even if they do not have a pure Ω character. States with $|\Omega| = 0$, 1, 2 are called Σ, Π, and Δ states, respectively, to parallel the diatomic molecule case. As ammonia has been shown[8,9] to behave as a nearly free rotor in the complex, all states of the van der Waals complex can be correlated with rotational states of NH_3 and the free rotor quantum numbers j and k can also be used to label the states of the complex. Finally, the states are also labeled by the number of quanta of excitation in the van der Waals stretch v_s. So, for example, the state $\Sigma\, 1_0(v_s = 1)$ is a state with $\Omega = 0$ that correlates to the $j_k = 1_0$ state of free NH_3 with one quantum of excitation in the vdW stretch coordinate.

In contrast with ortho NH_3–Ar, where the levels of A_1 symmetry in D_{3h}(M) are Pauli forbidden and only one level of each inversion tunneling doublet can actually be observed, both components of the inversion tunneling doublets occur in para NH_3–Ar. They are labeled as s (symmetric) and a (antisymmetric) according to their behavior under NH_3 inversion. In addition, all states with $|\Omega| > 0$ have two components that we denote (following the spectroscopic notation) as "upper" (u) and "lower" (l) states.

The eigenstates of the Hamiltonian (5) were obtained by a variational method with the basis of functions

$$|j, k, J, M, \Omega, n\rangle = \left[\frac{(2j+1)(2J+1)}{32\pi^3}\right]^{1/2} D^{(j)*}_{\Omega k}(0, \theta, \varphi)^* \times D^{(J)*}_{M\Omega}(\alpha, \beta, \gamma)^* \frac{\chi_n(R)}{R}\Phi^{\pm}_v(\rho), \quad (7)$$

where D denotes the Wigner functions and the angles (α, β, γ) are the overall rotation angles of the complex. β and α are the polar angles of the vector $\mathbf{R}$ with respect to the space-fixed frame and γ describes the rotation of the dimer about $\mathbf{R}$. The subscript v in $\Phi^{\pm}_v(\rho)$ denotes the umbrella vibrational quantum number and the superscript $\pm$ labels the umbrella tunneling components, while $\chi_n(R)/R$ is a complete set of radial functions. The functions $\Phi^{\pm}_v(\rho)$ were obtained by solving the one-dimensional Schrödinger equation with the Hamiltonian $\hat{H}_a$ of Eq. (6) in a sinc function discrete variable representation.[49,50] The functions $\chi_n(R)$ were obtained similarly, from the radial kinetic energy operator [the second term in Eq. (5)] and an effective radial potential $V_{\text{eff}}(R)$ of the form[51]

$$V_{\text{eff}}(R) = \alpha[V_0(R) + \zeta R]. \quad (8)$$

This potential consists of $V_0(R)$, a cut through the minimum of the 4D PES for angles $\rho = \rho_e$, $\theta = 85°$, and $\varphi = 60°$, supplemented with a linear term with slope ζ and a scaling factor α. The parameters α and ζ were optimized by minimizing the energy of the lowest rovibrational state of the NH_3–Ar

This article is copyrighted as indicated in the article. Reuse of AIP content is subject to the terms at: http://scitation.aip.org/termsconditions. Downloaded to IP: 164.15.19.51 On: Mon, 08 Dec 2014 14:51:09

complex with five eigenfunctions $\chi_n(R)$. The final values are $\alpha = 0.7$ and $\zeta = 4 \times 10^{-4}$ hartree/a_0.

The final calculation of the rovibrational bound states was performed in a basis with $j_{\max} = 10$, four umbrella functions, and 20 functions $\chi_n(R)$ calculated on an equidistant grid of 110 points from 4.5 to 20 a_0. Increasing $j_{\max}$ to 11 only changes the energy of the levels by about 10^{-5} cm^{-1}, while using 25 radial functions instead of 20 lowers the energy by about 10^{-6} cm^{-1}. The masses are 1.007825 u for H, 2.014102 u for D, 14.003074 u for ^{14}N, and 39.962383 u for ^{40}Ar. For each irreducible representation of the molecular symmetry group D_{3h}(M), we calculated the lowest 20 eigenvalues of the Hamiltonian with J ranging from 0 to 10 by means of the iterative algorithm of Davidson.[52]

The energies of the levels were subsequently fitted to the standard expression

$$E_J = E_0 + BJ(J+1) - DJ^2(J+1)^2 + HJ^3(J+1)^3, \tag{9}$$

in which E_0 is the band origin and the parameters B, D, and H are the rotational and distortion constants. Note that for states with $|\Omega| > 0$, the band origin is not the energy of the lowest level but the energy extrapolated to $J = 0$.

B. Results and discussion

1. NH_3–Ar

Before describing the bound states of the complex, it is instructive to inspect the anisotropy of the PES. It can be illustrated through the expansion coefficients $v_{lm}(R, \rho)$, see Eq. (3), shown in Fig. 5 for the equilibrium angle $\rho = \rho_e$. The isotropic potential v_{00} has a minimum at $R = 7.23$ a_0 and a depth of 109.8 cm^{-1}. These values are in very good agreement with those obtained from recent molecular beam experiments[1] (7.24 a_0 and 109.7 cm^{-1}, respectively). The depth of the isotropic potential v_{00} is thus substantially smaller than the well depth of the full potential (147.6 cm^{-1}). The dominant anisotropic terms are $v_{10}(R)$ and $v_{33}(R)$, as was previously noted.[18]

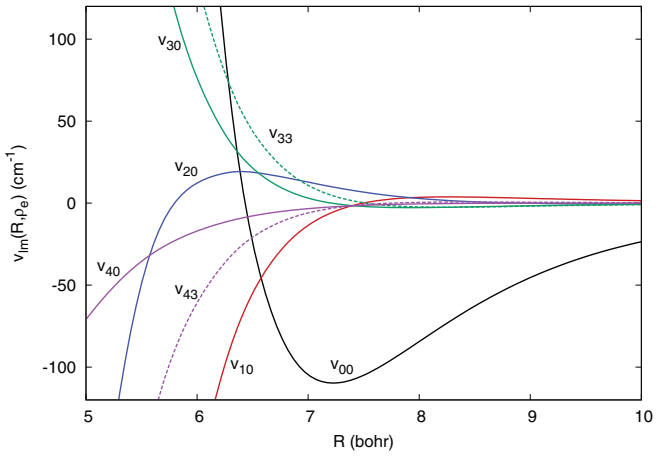

FIG. 5. Coefficients $v_{lm}(R, \rho)$ up to $l = 4$ as a function of the internuclear distance R for the equilibrium angle $\rho = \rho_e$.

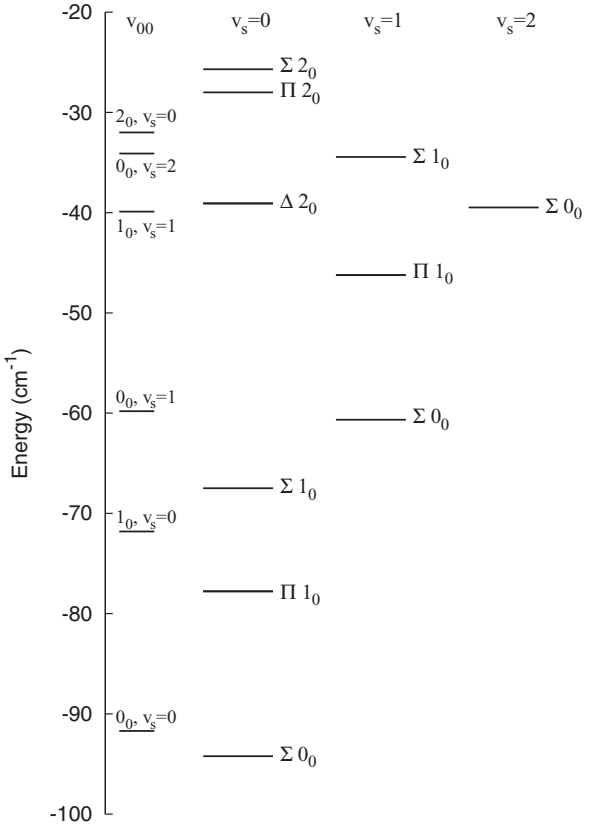

FIG. 6. Calculated vibrational levels of ortho NH_3–Ar. The states are distinguished by the value of v_s, the quantum number associated with vibration of the vdW stretch. The energies in the leftmost column are obtained from the isotropic potential $v_{00}(R)$, which makes the correlation of vdW states to the free rotor levels easier to see.

In order to interpret the spectrum, we first computed the vibrational spectrum obtained from the isotropic potential $v_{00}(R, \rho_e)$ using a B-splines method.[53] For each j_k level of NH_3, we obtained the energy of the various stretching excitations v_s. For example, for $j_k = 0_0$, the $v_s = 0$ state has an energy of -91.7 cm^{-1}, while the first and second excited states with $v_s = 1$ and $v_s = 2$ are at -58.9 cm^{-1} and -34.1 cm^{-1}, respectively. The energies of states with other values of j and k can be obtained in the same way. These results are shown in the leftmost column of Figs. 6 and 7 for ortho and para states, respectively.

Let us now discuss the results obtained from the full 4D calculations with the anisotropic potential. The band origins of the vibrational states of ortho NH_3–Ar up to an energy of -25 cm^{-1} are shown in Fig. 6. As was noted previously, NH_3 is nearly freely inverting in these states of the complex and it is possible to correlate the states of the complex with those of free NH_3. The band origins E_0, rotational constants B, and distortion constants D obtained from the fit (9) are given in Table III for all states and compared to the available experimental data. The energies E_0 are given with respect to the ground rovibrational state $\Sigma 0_0$ which is located at -94.22 cm^{-1}. It should be noted that states for which v_s is not listed correspond to the ground vdW stretch state $v_s = 0$. For the seven ortho states that have been reported in the literature,[6–8] we observe excellent agreement with our

This article is copyrighted as indicated in the article. Reuse of AIP content is subject to the terms at: http://scitation.aip.org/termsconditions. Downloaded to IP: 164.15.19.51 On: Mon, 08 Dec 2014 14:51:09

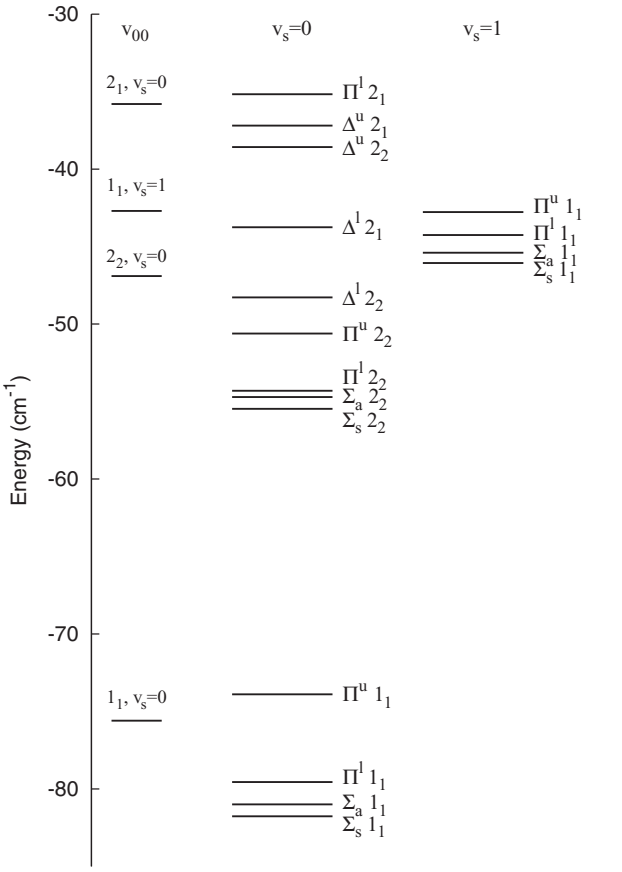

FIG. 7. Calculated vibrational levels of para NH_3–Ar. The states are distinguished by the value of v_s, the quantum number associated with vibration of the vdW stretch. The energies in the leftmost column are obtained from the isotropic potential $v_{00}(R)$, which makes the correlation of vdW states to the free rotor levels easier to see. The *a*/*s* splitting due to tunneling is too small to be seen for states with $\Omega \neq 0$.

calculations. The energies E_0 are all reproduced to within 0.75 cm^{-1}, the largest difference occurring for the $\Sigma\, 0_0(v_s = 1)$ state. The rotational constants B deviate by at most 2% from the experimental values. The agreement between the rotational constants D is good for the Σ and Π states, but large discrepancies occur for the Δ states.

If Ω were a good quantum number, the ortho states with $|\Omega| > 0$ would come in pairs of degenerate states. However, a small splitting occurs due to the Coriolis interaction, as was noted in Ref. 18. While the band origins are identical for the two components of these states, the rotational constants are slightly different (see Table III).

The vibrational states of para NH_3–Ar are shown in Fig. 7 up to an energy of -35 cm^{-1}. As for the ortho states, we observe a clear correlation between the states of the complex and the states of free NH_3. The band origins E_0 and the rotational and distortion constants B and D are reported in Table IV for these states and compared to the available experimental data. The energies E_0 are given with respect to the lowest rovibrational state of para NH_3–Ar ($\Sigma 1_1$), which is located at -81.77 cm^{-1}. Since the lowest level of free para NH_3, the 1_1^+ level, has energy 16.24 cm^{-1}, this implies that the dissociation energy $D_0 = 98.01$ cm^{-1} of para NH_3–Ar is higher than the value of $D_0 = 94.22$ cm^{-1} for ortho NH_3–Ar. A similar result was found for H_2O–H_2 in Ref. 51. The two pairs of states $\Sigma\, 1_1$ and $\Pi'\, 1_1$ are strongly mixed by the Coriolis interaction, and it was found better to fit the energies of both states simultaneously.[9] In order to compare with the experimental data, the values reported in Table IV are thus the average values $(B_\Sigma + B_\Pi)/2$ and $(D_\Sigma + D_\Pi)/2$ of the rotational constants.

As in the case of the ortho states, we find excellent agreement with the experimental data for the energies E_0,

TABLE III. Band origins E_0 (relative to the ground state energy of -94.22 cm^{-1}) and rotational and distortion constants B and D obtained from the fit, Eq. (9), for the states of ortho NH_3–Ar shown in Fig. 6, and comparison with experimental data.

	Symmetry	E_0 (cm^{-1})		B (MHz)		D (kHz)	
State	Even/odd J	Calc.	Expt.	Calc.	Expt.	Calc.	Expt.
$\Sigma\, 0_0$	A_2''/A_2'	0	0	2857.2	2876.8[a]	88.5	88.4[a]
$\Pi\, 1_0$	A_2''/A_2'	16.45	16.42[a]	2786.9	2801.9[a]	89.0	90.5[a]
$\Pi\, 1_0$	A_2'/A_2''	16.45	16.42[a]	2874.6	2890.7[a]	86.6	87.1[a]
$\Sigma\, 1_0$	A_2''/A_2'	26.74	26.47[b]	2807.6	2752.1[b]	111	107[b]
$\Sigma\, 0_0(v_s = 1)$	A_2''/A_2'	33.57	34.32[b]	2654.7	2660.4[b]	96.3	111[b]
$\Pi\, 1_0(v_s = 1)$	A_2''/A_2'	47.99		2661.4		104	
$\Pi\, 1_0(v_s = 1)$	A_2'/A_2''	47.99		2575.7		106	
$\Sigma\, 0_0(v_s = 2)$	A_2''/A_2'	54.74		2457.3		244	
$\Delta\, 2_0$	A_2''/A_2'	55.14	54.84[c]	2813.2	2833.0[c]	138	112[c]
$\Delta\, 2_0$	A_2'/A_2''	55.14	54.84[c]	2812.6	2836.1[c]	105	509[c]
$\Sigma\, 1_0(v_s = 1)$	A_2''/A_2'	59.77		2507.4		7.13	
$\Pi\, 2_0$	A_2''/A_2'	66.19		1896.0		–4911	
$\Pi\, 2_0$	A_2'/A_2''	66.21		2835.3		96.0	
$\Sigma\, 2_0$	A_2''/A_2'	68.50		3638.4		4610	

[a]Values from Ref. 6.
[b]Values from Ref. 7.
[c]Values from Ref. 8.

This article is copyrighted as indicated in the article. Reuse of AIP content is subject to the terms at: http://scitation.aip.org/termsconditions. Downloaded to IP: 164.15.19.51 On: Mon, 08 Dec 2014 14:51:09

TABLE IV. Band origins E_0 (relative to the ground state energy of -81.77 cm^{-1}) and rotational and distortion constants B and D obtained from the fit, Eq. (9), for the states of para NH_3–Ar shown in Fig. 7, and comparison with experimental data.

	Symmetry	E_0 (cm^{-1})		B (MHz)		D (kHz)	
State	Even/odd J	Calc.	Expt.	Calc.	Expt.	Calc.	Expt.
$\Sigma_s\,1_1$	E'/E''	0	0	2859.6	2881.0[a]	89.9	95.8[a]
$\Pi_s^l\,1_1$	E'/E''	2.2126	1.5103[b]				
$\Sigma_a\,1_1$	E''/E'	0.7697	0.7569[b]	2847.8	2872.7[a]	80.9	100.5[a]
$\Pi_a^l\,1_1$	E''/E'	2.2142	1.5103[b]				
$\Pi_s^u\,1_1$	E'/E''	7.8754	8.3858[b]	2847.3	2854.8[b]	69.1	72.4[b]
$\Pi_a^u\,1_1$	E''/E'	7.8754	8.3858[b]	2869.9	2872.3[b]	58.2	63.8[b]
$\Sigma_s\,2_2$	E'/E''	26.30		2147.1		− 3492	
$\Sigma_a\,2_2$	E''/E'	27.06		1955.0		− 6672	
$\Pi_s^l\,2_2$	E'/E''	27.47		3127.0		3308	
$\Pi_a^l\,2_2$	E''/E'	27.51		3259.1		5580	
$\Pi_s^u\,2_2$	E'/E''	31.161	31.266[c]	2650.0	2661.5[c]	184	189[c]
$\Pi_a^u\,2_2$	E''/E'	31.161	31.266[c]	2668.3	2681.3[c]	296	201[c]
$\Delta_s^l\,2_2$	E'/E''	33.49		2975.1		640	
$\Delta_a^l\,2_2$	E''/E'	33.49		2974.5		629	
$\Sigma_s\,1_1(v_s=1)$	E'/E''	35.712	35.807[c]	2855.2	2852.1[c]	− 346	− 169[c]
$\Sigma_a\,1_1(v_s=1)$	E''/E'	36.372	36.412[c]	2832.8	2822.8[c]	− 360	− 1098[c]
$\Pi_s^l\,1_1(v_s=1)$	E'/E''	37.516	37.507[c]	2664.5	2735.8[c]	− 50.7	165[c]
$\Pi_a^l\,1_1(v_s=1)$	E''/E'	37.515	37.507[c]	2630.7	2706.8[c]	− 155	106[c]
$\Delta_s^l\,2_1$	E'/E''	38.018	37.181[c]	2851.6	2827.0[c]	332	300[c]
$\Delta_a^l\,2_1$	E''/E'	38.019	37.181[c]	2849.8	2827.4[c]	404	284[c]
$\Pi_s^u\,1_1(v_s=1)$	E'/E''	38.995	39.413[c]	2669.7	2686.0[c]	− 19.7	25[c]
$\Pi_a^u\,1_1(v_s=1)$	E''/E'	38.995	39.413[c]	2725.1	2727.9[c]	76.5	90[c]
$\Delta_s^u\,2_2$	E'/E''	43.19		2816.3		95.8	
$\Delta_a^u\,2_2$	E''/E'	43.19		2816.1		77.8	
$\Delta_s^u\,2_1$	E'/E''	44.577	44.938[c]	2713.8	2728.8[c]	257	264[c]
$\Delta_a^u\,2_1$	E''/E'	44.577	44.938[c]	2713.7	2729.2[c]	211	263[c]
$\Pi_s^l\,2_1$	E'/E''	46.606	46.397[d]	2526.9	2925.9[d]	− 73.4	− 121[d]
$\Pi_a^l\,2_1$	E''/E'	46.606	46.397[d]	2651.1	2907.2[d]	317	− 189[d]

[a]Values from Ref. 9. The $\Sigma\,1_1$ and $\Pi^l\,1_1$ states are strongly coupled through the Coriolis interaction and the reported rotational constants are actually the average of the constants of the Σ and Π states.
[b]Values from Ref. 9.
[c]Values from Ref. 8.
[d]Values from Ref. 10.

the largest deviation being 0.84 cm^{-1}. The rotational constants are all reproduced to within 4%, except for the two $\Pi\,2_1$ states. However, it should be noted that the experimental determination of the rotational constants for these states[10] was obtained from a combined fit over several levels strongly coupled by Coriolis interaction, which makes a direct comparison difficult. The comparison of the rotational constants D shows some large differences, particularly for the higher lying states.

As was discussed above, the para states of NH_3–Ar are split into doublets by the inversion tunneling of NH_3. However, the tunneling in the complex is quite different than for free NH_3 as the Ar atom perturbs the double well potential of NH_3. Inversion of NH_3 in the complex corresponds to the transformation $\theta \rightarrow \pi - \theta$, and it was found in Sec. II B that there is a 13.5 cm^{-1} difference between the minima of the configurations $\theta = 0$ and $\theta = 180^\circ$ for $\rho = \rho_e$. This difference is much larger than the 0.79 cm^{-1} splitting corresponding to tunneling in free NH_3. Tunneling is therefore quenched almost completely in the para states of the complex, except for $\Omega = 0$ (Σ) states for which the wave function is symmetric with respect to $\theta = \pi/2$. It is thus expected that the tunneling splitting in Σ states will be similar to that of free NH_3, while for the $|\Omega| > 0$ states it almost vanishes.[9,16,25] From Table IV we see that the splittings in the band origin ($J = 0$) of the Σ states are 0.77 cm^{-1}, 0.66 cm^{-1}, and 0.76 cm^{-1} for the $\Sigma\,1_1$, $\Sigma\,1_1(v_s = 1)$, and $\Sigma\,2_2$ states, respectively. For the Π and Δ states, the tunneling splitting in the band origin is indeed negligibly small, but there is a small splitting between the rotational levels due to the Coriolis interaction, as was already shown by van Bladel *et al.*[18] This splitting increases with J.

In earlier calculations of the low-lying rovibrational states of the NH_3–Ar complex[17] with the potential of Ref. 16 discrepancies with the experimental data were observed. For instance, in ortho NH_3–Ar the splitting between the two states correlating to the 1_0 state of free ammonia was much too small, while in para NH_3–Ar the ground state was predicted to be a state with $|\Omega| = 1$, in contradiction to the experimental data. It was shown[18,19] that the agreement with the experimental data could be improved by scaling the $v_{33}(R)$ term in the expansion of the potential by a single parameter. We observe that with our new potential energy surface, without any scaling, the energies

This article is copyrighted as indicated in the article. Reuse of AIP content is subject to the terms at: http://scitation.aip.org/termsconditions. Downloaded to IP: 164.15.19.51 On: Mon, 08 Dec 2014 14:51:09

TABLE V. Band origins E_0 (relative to the ground state energy of -98.23 cm^{-1}) and rotational and distortion constants B and D obtained from the fit, Eq. (9), for the lowest lying states of ortho and para ND_3–Ar and comparison with experimental data.

	Symmetry	E_0 (cm^{-1})		B (MHz)		D (kHz)	
State	Even/odd J	Calc.	Expt.	Calc.	Expt.	Calc.	Expt.
$\Sigma_s\,0_0$	A_1'/A_1''	0		2583.9	2601.0[a]	69.9	69.3[a]
$\Sigma_a\,0_0$	A_2''/A_2'	0.0485	0.0479[b]	2583.9	2601.0[a]	69.9	69.3[a]
$\Pi_s^l\,1_0$	A_2''/A_2'	7.6904	7.8113[b]	2543.5	2618.4[b]	74.8	73.9[b]
$\Pi_s^u\,1_0$	A_2'/A_2''	7.6904	7.8113[b]	2602.0	2618.4[b]	66.8	66.1[b]
$\Pi_a^l\,1_0$	A_1'/A_1''	7.7407	7.8593[b]	2543.4	2618.4[b]	74.8	73.9[b]
$\Pi_a^u\,1_0$	A_1''/A_1'	7.7407	7.8593[b]	2602.0	2618.4[b]	66.8	66.1[b]
$\Sigma_s\,1_0$	A_2''/A_2'	20.718	20.104[c]	2540.8		65.6	
$\Sigma_a\,1_0$	A_1'/A_1''	20.762	20.141[c]	2540.9		65.7	
$\Sigma_s\,1_1$	E'/E''	5.1527	5.2008[c]	2446.7	2449.0[a]	− 148.7	− 163.7[a]
$\Sigma_a\,1_1$	E''/E'	5.2033	5.2506[c]	2445.7	2447.4[a]	− 155.0	− 171.6[a]
$\Pi_s^l\,1_1$	E''/E'	7.3566		2699.5		299.5	
$\Pi_a^l\,1_1$	E'/E''	7.3566		2699.7		293.0	
$\Pi_s^u\,1_1$	E'/E''	10.721		2590.8		69.1	
$\Pi_a^u\,1_1$	E''/E'	10.721		2592.1		68.9	

[a]Values from Ref. 12.
[b]Values from Ref. 14.
[c]Values computed from the PES of Schmuttenmaer *et al.*[25] fitted from spectroscopic data.

of the levels are in complete agreement with the experiment.

2. ND_3–Ar

The spectrum of ND_3–Ar has been the subject of three studies.[12–14] The main difference compared to NH_3–Ar is that the total wave function must now be symmetric with respect to the permutation of the D nuclei that have a spin $I = 1$, which results in the fact that the rovibrational states have nonzero nuclear spin statistical weights for all irreducible representations of the D_{3h}(M) group.[48]

We have computed the first 20 eigenvalues of the Hamiltonian for each irreducible representation with J ranging from 0 to 10 using the method outlined above. Convergence was obtained with $j_{\max} = 11$ and a grid of 120 points ranging from 4.5 a_0 to 20 a_0, all other parameters of the calculations being identical to the NH_3–Ar case. The band origins E_0 and the rotational and distortion constants B and D are presented in Table V for the states of all the nuclear spin species of ND_3–Ar correlating to the $j_k = 0_0$, 1_0, and 1_1 levels of ND_3, together with the available experimental data. The energies are given with respect to the ground rovibrational state $\Sigma_s\,0_0$, located at -98.23 cm^{-1}. The inversion splitting in the $\Sigma\,0_0$ state is 0.0485 cm^{-1}, close to that of free ND_3, 0.0530 cm^{-1}. The splitting is 0.0503 cm^{-1} in the $\Pi\,1_0$ states while it is 0.0441 cm^{-1} in the $\Sigma\,1_0$ states and 0.0506 cm^{-1} in the $\Sigma\,1_1$ states. On the other hand, for the Π states of E symmetry, the splitting is almost completely quenched, as was found for NH_3–Ar.

We find excellent agreement with the experimental data for the energies E_0 as well as for the rotational constants. It should be noted that the experimental values for the energies of the $\Sigma_a\,0_0$ and all the $\Pi\,1_0$ states were obtained by assuming that the inversion splitting is the same in the Σ and Π states,[14] which is a reasonable assumption, as confirmed by our calculations. In the case of the $\Pi\,1_0$ states, we obtain two sets of states with the same band origin, but different rotational constants B and D due to the effect of Coriolis couplings. On the other hand, the values of B and D are identical for the symmetric (s) and antisymmetric (a) tunneling component of each state. Melnik *et al.*[14] obtained a single value of B for all $\Pi\,1_0$ states, while we find a small difference of 59 MHz between the two components of the Π states. For the $\Sigma\,1_1$ states, we find again excellent agreement with the experimental data. The band origins were obtained by Schmuttenmaer *et al.*[25] from their experimentally determined PES. The $\Sigma\,1_1$ states are strongly perturbed by Coriolis interactions as in the case of NH_3–Ar, which is reflected by the negative values of the D constants.

IV. CONCLUSIONS

We have constructed a new 4D PES for the interaction of NH_3 with Ar using the CCSD(T) method and the aug-cc-pVQZ basis set supplemented with midbond functions. The PES depends on the umbrella coordinate of NH_3 and describes its inversion motion. The PES was accurately fitted to an analytical form including a correct description of its long range behavior and its properties were investigated. We found that the global minimum of the PES has a depth of 147.64 cm^{-1} and that the equilibrium geometry agrees very well with a prediction based on spectroscopic data.

We investigated the rovibrational spectrum of the NH_3–Ar complex including the effects of the umbrella motion as well as the Coriolis interaction. Using a variational method combined with a discrete variable representation, we computed the rovibrational and inversion tunneling states of the complex for values of the total angular momentum $J = 0 - 10$. The dissociation energy D_0 equals 94.22 cm^{-1} for ortho NH_3–Ar and 98.01 cm^{-1} for para NH_3–Ar. The experimental band origins of all the rovibrational states of ortho

This article is copyrighted as indicated in the article. Reuse of AIP content is subject to the terms at: http://scitation.aip.org/termsconditions. Downloaded to IP: 164.15.19.51 On: Mon, 08 Dec 2014 14:51:09

NH_3–Ar are reproduced to within 0.75 cm^{-1} and the rotational constants B differ by at most 2% from the experimental values. For para NH_3–Ar, the maximum deviation is 0.84 cm^{-1} for the band origins and 4% for the constants B. We confirmed the observation that the tunneling splitting is only slightly smaller than that of free NH_3 for the states of ortho NH_3–Ar and for the Σ states of para NH_3–Ar, while it is nearly quenched for para NH_3–Ar states with $|\Omega| > 0$.

We also computed the lowest rotational states of ND_3–Ar and again obtained excellent agreement with the spectroscopic data. The dissociation energies D_0, 98.23 cm^{-1} for the A_1 and A_2 symmetry species and 101.32 cm^{-1} for the E species, are slightly larger than those of NH_3–Ar. The inversion tunneling splittings show qualitatively the same behavior as for NH_3–Ar, although they are substantially smaller (as in free ND_3 in comparison with free NH_3).

We conclude that the agreement shown with experimental data demonstrates the accuracy of the present potential energy surface, which will also be used for scattering calculations.

ACKNOWLEDGMENTS

All the calculations presented in this work were performed on the Hydra cluster at the ULB/VUB Computing Center. This work was supported by the Fonds de la Recherche Scientifique – FNRS and by the Wiener-Anspach Foundation.

[1]F. Pirani, L. Roncaratti, L. Belpassi, F. Tarantelli, and D. Cappelletti, J. Chem. Phys. **135**, 194301 (2011).
[2]B. Yang and P. C. Stancil, Eur. Phys. J. D **47**, 351 (2008).
[3]P. Żuchowski and J. M. Hutson, Phys. Rev. A **78**, 022701 (2008).
[4]G. Fraser, D. Nelson, Jr., A. Charo, and W. Klemperer, J. Chem. Phys. **82**, 2535 (1985).
[5]D. Nelson, Jr., G. Fraser, K. I. Peterson, K. Zhao, and W. Klemperer, J. Chem. Phys. **85**, 5512 (1986).
[6]E. Zwart and W. Meerts, Chem. Phys. **151**, 407 (1991).
[7]C. Schmuttenmaer, R. Cohen, J. Loeser, and R. Saykally, J. Chem. Phys. **95**, 9 (1991).
[8]C. Schmuttenmaer, J. Loeser, and R. Saykally, J. Chem. Phys. **101**, 139 (1994).
[9]E. Zwart, H. Linnartz, W. Meerts, G. Fraser, D. Nelson, Jr., and W. Klemperer, J. Chem. Phys. **95**, 793 (1991).
[10]A. Grushow, W. Burns, S. Reeve, M. Dvorak, and K. Leopold, J. Chem. Phys. **100**, 2413 (1994).
[11]K. Didriche, T. Földes, T. Vanfleteren, and M. Herman, J. Chem. Phys. **138**, 181101 (2013).
[12]J. van Wijngaarden and W. Jäger, J. Chem. Phys. **114**, 3968 (2001).
[13]D. Melnik, S. Gopalakrishnan, T. Miller, F. De Lucia, and S. Belov, J. Chem. Phys. **114**, 6100 (2001).
[14]D. Melnik, T. Miller, and F. De Lucia, J. Mol. Spectrosc. **214**, 202 (2002).
[15]G. Chalasinski, S. Cybulski, M. Szczesniak, and S. Scheiner, J. Chem. Phys. **91**, 7809 (1989).
[16]M. Bulski, P. Wormer, and A. van der Avoird, J. Chem. Phys. **94**, 491 (1991).
[17]J. van Bladel, A. van der Avoird, and P. Wormer, J. Chem. Phys. **94**, 501 (1991).
[18]J. van Bladel, A. van der Avoird, and P. Wormer, J. Phys. Chem. **95**, 5414 (1991).
[19]J. van Bladel, A. van der Avoird, and P. Wormer, Chem. Phys. **165**, 47 (1992).
[20]J. Schleipen, J. ter Meulen, G. van der Sanden, P. Wormer, and A. van der Avoird, Chem. Phys. **163**, 161 (1992).
[21]G. van der Sanden, P. Wormer, A. van der Avoird, J. Schleipen, and J. ter Meulen, J. Chem. Phys. **97**, 6460 (1992).
[22]G. van der Sanden, P. Wormer, A. van der Avoird, C. Schmuttenmaer, and R. Saykally, Chem. Phys. Lett. **226**, 22 (1994).
[23]G. van der Sanden, P. Wormer, and A. van der Avoird, J. Chem. Phys. **105**, 3079 (1996).
[24]F.-M. Tao and W. Klemperer, J. Chem. Phys. **101**, 1129 (1994).
[25]C. Schmuttenmaer, R. Cohen, and R. Saykally, J. Chem. Phys. **101**, 146 (1994).
[26]G. Bistoni, L. Belpassi, F. Tarantelli, F. Pirani, and D. Cappelletti, J. Phys. Chem. A **115**, 14657 (2011).
[27]J. Kay, S. Y. T. van de Meerakker, E. Wade, K. Strecker, and D. Chandler, J. Phys. Chem. A **113**, 14800 (2009).
[28]O. Tkac, A. K. Saha, J. Onvlee, C.-H. Yang, G. Sarma, C. K. Bishwakarma, S. Y. T. van de Meerakker, A. van der Avoird, D. H. Parker, and A. J. Orr-Ewing, Phys. Chem. Chem. Phys. **16**, 477 (2014).
[29]K. B. Gubbels, S. Y. T. van de Meerakker, G. C. Groenenboom, G. Meijer, and A. van der Avoird, J. Chem. Phys. **136**, 074301 (2012).
[30]S. Yu, J. C. Pearson, B. J. Drouin, K. Sung, O. Pirali, M. Vervloet, M.-A. Martin-Drumel, C. P. Endres, T. Shiraishi, K. Kobayashi, and F. Matsushima, J. Chem. Phys. **133**, 174317 (2010).
[31]X. Huang, D. W. Schwenke, and T. J. Lee, J. Chem. Phys. **129**, 214304 (2008).
[32]C. Hampel, K. Peterson, and H. J. Werner, Chem. Phys. Lett. **190**, 1 (1992).
[33]H.-J. Werner, P. J. Knowles, G. Knizia, F. R. Manby, M. Schütz *et al.*, MOLPRO, version 2012.1, a package of *ab initio* programs, 2012, see http://www.molpro.net.
[34]S. F. Boys and F. Bernardi, Mol. Phys. **19**, 553 (1970).
[35]T. H. Dunning, Jr., J. Chem. Phys. **90**, 1007 (1989).
[36]D. E. Woon and J. T. H. Dunning, J. Chem. Phys. **98**, 1358 (1993).
[37]T. Helgaker, P. Jørgensen, and J. Olsen, *Molecular Electronic Structure Theory* (John Wiley and Sons, NJ, 2000).
[38]S. M. Cybulski and R. R. Toczylowski, J. Chem. Phys. **111**, 10520 (1999).
[39]A. Wolf, M. Reiher, and B. Hess, J. Chem. Phys. **117**, 9215 (2002).
[40]W. de Jong, R. Harrison, and D. Dixon, J. Chem. Phys. **114**, 48 (2001).
[41]C. Lauzin, E. Cauët, J. Demaison, M. Herman, H. Stoll, and J. Liévin, Mol. Phys. **110**, 2751 (2012).
[42]T. H. Dunning, Jr., K. Peterson, and A. Wilson, J. Chem. Phys. **114**, 9244 (2001).
[43]K. Peterson and T. H. Dunning, Jr., J. Chem. Phys. **117**, 10548 (2002).
[44]J. Loreau, H. R. Sadeghpour, and A. Dalgarno, J. Chem. Phys. **138**, 084301 (2013).
[45]See supplementary material at http://dx.doi.org/10.1063/1.4903047 for the *ab initio* data points.
[46]T. J. Lee, Chem. Phys. Lett. **372**, 362 (2003).
[47]A. van der Avoird, P. Wormer, F. Mulder, and R. Berns, Top. Curr. Chem. **93**, 1 (1980).
[48]P. R. Bunker and P. Jensen, *Molecular Symmetry and Spectroscopy*, 2nd ed. (NRC Research Press, Ottawa, 1998).
[49]D. T. Colbert and W. H. Miller, J. Chem. Phys. **96**, 1982 (1992).
[50]G. C. Groenenboom and D. T. Colbert, J. Chem. Phys. **99**, 9681 (1993).
[51]A. van der Avoird and D. Nesbitt, J. Chem. Phys. **134**, 044314 (2011).
[52]E. R. Davidson, J. Comput. Phys. **17**, 87 (1975).
[53]J. Loreau, J. Liévin, and N. Vaeck, J. Chem. Phys. **133**, 114302 (2010).

This article is copyrighted as indicated in the article. Reuse of AIP content is subject to the terms at: http://scitation.aip.org/termsconditions. Downloaded to IP: 164.15.19.51 On: Mon, 08 Dec 2014 14:51:09